ARTICLE   OPEN

Check for updates

Increased risk of flash droughts with raised concurrent hot and dry extremes under global warming

Zhaoqi Zeng[1,2,3,4], Wenxiang Wu [1,5 ✉], Josep Peñuelas [3,4 ✉], Yamei Li[5], Wenzhe Jiao[6], Zhaolei Li[7], Xinshuai Ren[1,2], Ke Wang[1,2] and Quansheng Ge[1 ✉]

Flash droughts pose large threats to crop yields and ecosystem services due to their sudden onset and rapid intensification, arousing wide public concern in a warming climate. Their long-term characteristics of change, underlying mechanisms, and especially potential impacts on agriculture, forests, and populations at a global scale, however, remain largely unknown. We used in situ observations, two observation-based global reanalysis data sets, and 22 Earth system models to determine that flash droughts are shifting toward more frequent, accelerated-onset, and longer duration. These changes increased the exposure of agricultural areas, forested areas, and populations to flash droughts by 20.3%, 17.1%, and 30.0%, respectively, during 2001–2020 compared to 1981–2000, with a disproportionate increase in integrated risks across the Amazon Basin and eastern and southern Asia. The increase in concurrent hot and dry climatic conditions driven by warming has been mostly responsible for enabling and intensifying flash droughts over large regions. State-of-the-art Coupled Model Intercomparison Project Phase 6 (CMIP6) models, however, failed to identify the acceleration of the onset time of flash droughts and widely underestimated the occurrence of flash droughts that are driven only by precipitation deficits or by heat waves, probably because they misrepresent the dependence between precipitation and temperature and underestimate the sensitivity of soil moisture to temperature and precipitation at short timescales (e.g., 5 days). These syntheses comprehensively advance our understanding of the characteristics and impacts of flash droughts but also highlight that the CMIP6 models need to be validated to represent the correct covariability between climatic variables at short timescales to provide more reliable projections of flash droughts.

npj Climate and Atmospheric Science (2023)6:134 ; https://doi.org/10.1038/s41612-023-00468-2

INTRODUCTION

Droughts have been, and will continue to be, large threats to agricultural, environmental, and even socioeconomic systems under global warming[1–4]. In the conventional notion, drought generally refers to a slow phenomenon attributable to a gradual accumulation of negative precipitation anomalies and may persist for several months or years[5,6]. Recent studies, however, have indicated that droughts can also develop unusually rapidly under extreme atmospheric conditions (e.g., precipitation deficits and heat waves) within a few pentads (i.e., 5 days) or weeks. The term "flash drought" has been coined to describe this type of drought with a rapid onset and intensification[7–10]. Compared with conventional slowly developing droughts, flash droughts often surprise stakeholders (e.g., farmers), leaving little time for drought preparation and mitigation and thus potentially causing more catastrophic impacts on the agricultural and ecological sectors[11,12]. For example, the 2012 flash drought in the central United States of America, which intensified rapidly from non-drought to extreme or exceptional drought conditions during the growing season, was one of the most expensive natural disasters in the country. Losses of more than $30 billion were attributed to this event, and the percentage of yield loss was one of the largest on record since 1866[13]. Eastern Australia also experienced a sudden shift from wet conditions in December 2017 to extremely dry conditions in January 2018. This rapid development of

drought led to widespread tree mortality and the smallest livestock populations in the country[14]. In particular, such "flash" extreme events may become more prevalent than expected, given that increasing atmospheric water demand and strengthening feedbacks between the land and atmosphere in a warming climate may further exacerbate the drying process in a faster and more intense manner[15,16]. Understanding the characteristics and drivers of flash droughts across regions and especially the exposure of human and natural systems to such extremes is thus urgently needed to form a basis for reducing vulnerability and to improve the mitigation and response capacities of people and systems at risk.

Precisely quantifying the development of flash droughts is prerequisite to effectively delineating the characteristics and assessing the impacts of drought. Recent studies have improved the monitoring of flash droughts by using a variety of indices, including the Standard Evaporative Stress Ratio[17], the Evaporative Stress Index[18,19], the integration of the Evaporative Stress Index and the Rapid Change Rate Index[20], the Evaporative Demand Drought Index[21], the Standardized Precipitation Index and the Standardized Evaporation Precipitation Index at short time-scales[22,23], the trajectory of solar-induced chlorophyll fluorescence[24], and anomalies in the soil moisture[15,16]. Among these indices, it is generally accepted that anomalies in soil moisture in the root zone have particular advantages in characterizing the

[1]Key Laboratory of Land Surface Pattern and Simulation, Institute of Geographic Sciences and Natural Resources Research, Chinese Academy of Sciences, Beijing 100101, China. [2]Department of Environment and Resources, University of Chinese Academy of Sciences, Beijing 100049, China. [3]CSIC, Global Ecology Unit CREAF-CSIC-UAB, Bellaterra 08193 CA, Spain. [4]CREAF, Cerdanyola del Vallès 08193 CA, Spain. [5]State Key Laboratory of Tibetan Plateau Earth System, Environment and Resources (TPESER), Institute of Tibetan Plateau Research, Chinese Academy of Sciences, Beijing 100101, China. [6]Department of Ecology and Conservation Biology, Texas A&M University, College Station, TX, USA. [7]College of Resources and Environment, and Academy of Agricultural Sciences, Southwest University, Chongqing 400715, China. ✉email: wuwx@igsnrr.ac.cn; Josep.Penuelas@uab.cat; geqs@igsnrr.ac.cn

onset and identifying the impacts of flash droughts because the root-zone soil moisture is highly sensitive to variabilities of other climatic factors (e.g., precipitation and temperature) and is a direct source of moisture for vegetation[25,26]. Several recent studies have thus focused on the evolution and long-term trend of regional and global flash droughts by using the root-zone soil moisture and found that human-induced climate change has greatly increased the frequency of flash droughts[16,27,28]. Especially, the speed of drought onset may also be accelerating, as a recent study suggests that a transition from slow to flash droughts has occurred on a global scale[29]. These studies provide a useful estimation of flash drought indices and a multi-faceted understanding of changing characteristics of flash droughts at regional and global scales, generally highlighting the role of anthropogenic warming in the long-term increasing trend of flash droughts over the past few decades.

However, it should be noted that the climatic background under anthropogenic warming may be quite different before and the after 2000, as several recent studies have reported that the atmospheric water demand (indicated by the vapor-pressure deficit [VPD] or potential evapotranspiration) has dramatically increased in the last two decades (i.e., after 2000) and that heat waves and their associated disturbances (e.g., precipitation and soil-moisture deficits) now occur more frequency than before[30–32]. Such exacerbated climatic aridification and increased perturbations associated with warming can not only accelerate the increasing trend of flash droughts by speeding up the soil moisture depletion, but may also increase the likelihood of flash droughts being evolved into long-term seasonal droughts through strengthening land–atmosphere feedbacks[8]. This suggests that the evolution, propagation, and even driving mechanisms of flash droughts may have changed considerably after 2000 and are expected to pose a greater threat to vegetation growth, crop yields, and even socioeconomic development. However, a comprehensive comparison of the changing characteristics and dominant drivers of flash droughts before and after 2000, as well as an improved quantification of drought impacts on natural and human systems at regional and global scales, is still missing. This knowledge gap hinders a deeper understanding of the physical mechanisms underlying changes in characteristics of flash drought in a warming climate and restricts our ability to inform assessments of the risks of flash droughts to interconnected systems and coping with their societal impacts.

To address these questions, we used in situ observations from 36 flux-tower sites, two global observation-based reanalysis soil-moisture data sets, and 22 Earth system models developed as part of the Coupled Model Intercomparison Project Phase 6 (CMIP6) to specifically (1) quantify the global and regional changes in the characteristics of flash droughts (e.g., frequency, duration, seasonality, and time of onset) between 1981–2000 and 2001–2020; (2) characterize the changes in exposure from such flash climatic shocks to agriculture, forests, and populations; (3) understand the role of precipitation deficits, positive temperature anomalies, and their combinations on the evolution of flash droughts; and (4) evaluate the ability of the CMIP6 models to simulate the characteristics and drivers of the occurrence of flash droughts. These investigations advance our understanding of the development, occurrence mechanisms, and impacts of flash droughts on a regional and global scale and provide a scientific basis for mitigating potential losses associated with flash droughts under global warming.

RESULTS

Definition and observed characteristics of flash droughts

To synthetically identify a flash drought and distinguish it from a long-term seasonal drought, we considered both the rapid rate of intensification and the duration of drought, as described by Yuan et al.[16] and Ford and Labosier[33], to define flash droughts: the pentad (5 days) soil moisture in the root zone decreases from above the 40th percentile to below the 20th percentile, with a mean rate of decrease no less than the 5th percentile for each pentad during the periods when droughts develop (i.e., decrease from t_0 to t_1 within 4 pentads; Fig. 1a). A flash drought will end when the low soil moisture increases again to greater than or equal to the 20th percentile. The time between the end of the period of drought development (t_1) and the termination of a flash drought is defined as the duration of the drought. The duration of a flash drought should be no less than three pentads to exclude dry spells that last for too short a period to have any impacts but should be less than 12 pentads (i.e., 2 months) to distinguish it from a long-term seasonal drought. A flash drought will develop into a long-term seasonal drought when the duration is longer than 12 pentads.

We used FLUXNET data to identify 393 flash droughts with durations of no less than three pentads by using daily soil-moisture observations from 473 site-years. The results indicated that the frequency of flash droughts has increased significantly ($p < 0.01$ based on Mann-Kendall test) in the last two decades, with most occurring in spring (27.2%) and summer (27.7%) and with relatively small probabilities of developing in winter (Fig. 1b, c). The flash droughts that developed in summer and autumn had high probabilities (16.2% and 27.6%, respectively) of evolving into long-term seasonal droughts relative to those that developed in spring and winter, potentially posing a far greater threat because of their rapid onsets and long durations. In particular, a large proportion of flash droughts developed within one (35.1%) and two (34.6%) pentads, suggesting that flash droughts have developed faster in the last two decades.

We also used two observation-based data sets of root-zone soil moisture to measure the global spatial and temporal changes in the characteristics of flash droughts during 1981–2020 (Fig. 2). Although soil moisture data remains uncertain in some regions (Supplementary Fig. 1), each dataset supports the fact that the frequency of, and areas affected by, flash droughts have increased greatly, especially during the last two decades, consistent with the FLUXNET results. The global mean percentage of flash droughts that developed within one pentad increased from 10% in the 1980s to more than 20% recently, and the number of flash droughts that developed within three and four pentads decreased substantially in recent decades for all two data sets (Fig. 2d and Supplementary Fig. 2). These findings further support the accelerating onset of flash droughts. Global accumulated occurrences of flash droughts that developed into long-term seasonal droughts have also increased two-fold in recent years compared to before the 2000s, with a surge after 2018 (Fig. 2e), causing a superimposed risk of flash droughts.

The areas prone to flash droughts were similar for 1981–2000 and 2001–2020 and were mainly in the Amazon Basin, southeastern North America, northern and central-eastern Europe, middle Africa, and southern and southeastern Asia (Fig. 2a, b). By comparison, the frequency of flash droughts in humid and vegetated regions, especially the Amazon Basin and middle Africa (e.g., Congo Basin), has increased greatly in the last two decades relative to 1981–2000 (Fig. 2c). These increases occurred mainly in late spring and early summer in the Northern Hemisphere but in late autumn and winter in the Southern Hemisphere (Fig. 2f, g). We detrended soil moisture using a linear method and reanalyzed our data to determine whether the increased frequency of flash droughts was caused by the long-term trend in soil moisture. The results were highly consistent with those from the non-detrended analysis during 2001–2020 (Supplementary Fig. 3), suggesting that the long-term trend in soil moisture contributed little to the faster, intensified development of flash droughts in recent two decades. Contrary to the non-detrended analysis, there is a clear decreasing
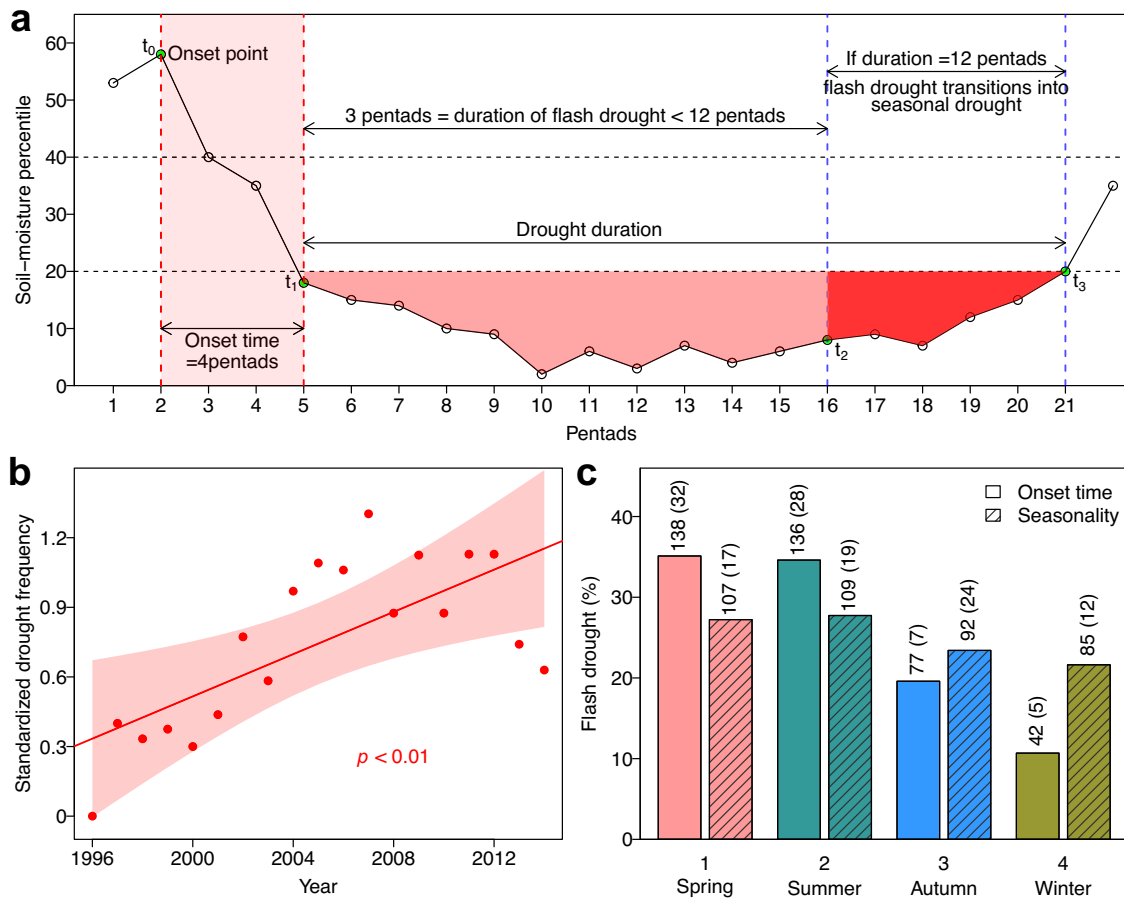
Fig. 1 Definition and characteristics of flash droughts. a Illustration of the definition of a flash drought. The five-day mean soil moisture decreases from above the 40th percentile to below the 20th percentile within 4 pentads (i.e., mean decline rate $\geq$5 percentile for each pentad), and then the soil moisture below the 20th percentile should last for no less than three pentads but no more than 12 pentads. If a flash drought lasts for more than 12 pentads, it develops into a long-term seasonal drought. The light-pink shaded area (from t_0 to t_1) represents the period of development of the flash drought, the dark-pink shaded area (from t_1 to t_2) represents the duration of the flash drought, and the red shaded area (from t_2 to t_3) indicates when the flash drought develops into a long-term seasonal drought. **b** The temporal changes in the normalized frequency of flash droughts during 1996–2014, and $p < 0.01$ indicates the statistically significant based on Mann-Kendall test, and **c** the percentage of flash droughts at different times of onset and in different seasons calculated by using FLUXNET data. The seasonal division of flash droughts are based on the period of their development (i.e., onset time); if a flash drought event develops in spring but persists into summer, we classify this event as a spring flash drought. The number represents the total occurrences of flash droughts and that developed into long-term season droughts.

trend in the occurrence of flash droughts that developed within one pentad before 2000 (Supplementary Fig. 3d). This likely indicates that the drying or wetting trend of soil moisture has a remarkable impact on the speed by which flash droughts develop during the period from 1981 to 2000.

Increasing exposure to flash droughts

We quantified the additional impacts of these more frequent, faster developing, and longer flash droughts on agricultural and forested areas and on populations by calculating the changes in their exposure to flash droughts in the last two decades compared with 1981–2000 (Fig. 3). The results indicated that the exposure of agricultural areas (i.e., the combination of pastureland and cropland) to flash droughts increased by 20.3% during 2001–2020 relative to 1981–2000 (Fig. 3a). Specifically, global averages of 5291 km² of cropland and 9345 km² of pastureland per year were exposed to flash droughts in the last two decades, compared with 4793 and 7374 km² per year, respectively, during 1981–2000. Forests faced more challenges than cropland from flash droughts under climate change: their exposure to flash droughts increased by 17.1% during 2001–2020 (11,292 km² per

year) relative to 1981–2000 (9649 km² per year). The increased exposure of agricultural and forested areas was mainly dominated by increases in the duration and frequency of flash droughts and the regions they affected because we did not account for changes in the agricultural and forested areas in the two periods when calculating exposure. The intensification of flash droughts also contributed to a large increase in population exposure in the last two decades. Specifically, the global mean population exposure increased by 30.0% during 2001–2020 relative to 1981–2000, increasing from 2.03 million to approximately 2.63 million people per year. The population also increased widely in the last two decades compared to 1981–2000, especially in central Africa, southeastern North America, and southern and southeastern Asia (Supplementary Fig. 4), which partially contributed to the recent dramatic increase in population exposure.

Forest exposure consistently increased at a regional scale between the two study periods in 18 Intergovernmental Panel on Climate Change (IPCC) regions (Fig. 3b and Supplementary Fig. 5), with a focus on the 26 largest geographical regions designated in recent IPCC reports (Supplementary Fig. 6)[34]. The foci of increases in forest exposure to flash droughts were mainly in the Amazon Basin (from 34,349 to 41,788 km² per year), western Africa (from
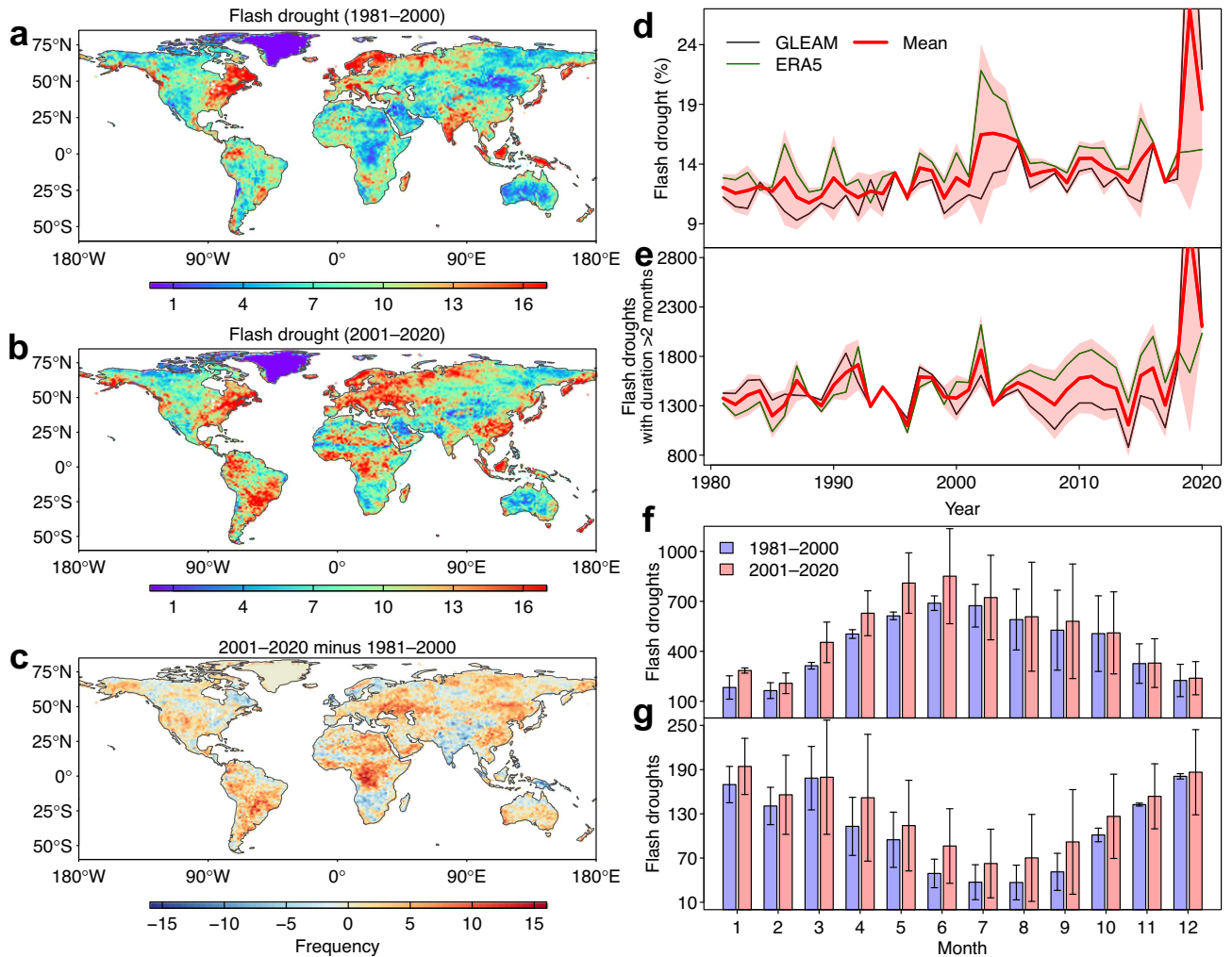
Fig. 2 Characteristics of flash droughts calculated according to two global observation-based datasets. Spatial patterns of the frequency of flash droughts during **a** 1981–2000 and **b** 2001–2020, and **c** their difference calculated by using the GLEAM and ERA5 datasets. **d** Temporal changes in the percentage of flash droughts that developed within one pentad, and **e** the accumulated times of flash droughts that developed into long-term seasonal droughts. The solid red line represents the mean of two different datasets, and the shaded areas represents the mean ±1 s.d. Monthly accumulated occurrences of flash droughts in the **f** Northern and **g** Southern Hemispheres. Error bars indicate ±1 standard error from the mean.

12,976 to 26,176 km² per year), eastern Africa (from 8089 to 14,350 km² per year), and central Europe (from 9174 to 13,038 km² per year). The relatively large increase in agricultural exposure to flash droughts occurred mainly in central Asia (from 25,522 to 34,833 km² per year), southeastern and south America (from 18,764 to 30,834 km² per year), the eastern Africa (from 23,489 to 31,656 km² per year), and central Europe (from 15,238 to 24,262 km² per year). South Europe/Mediterranean, central and northern America, and southern Africa also had high levels of agricultural exposure to flash droughts, but the exposed areas changed little or even decreased slightly in the last two decades. The exposure of populations to flash droughts increased considerably in the most densely populated areas, such as eastern Asia (from 7.9 to 12.2 million per year) and southeastern Asia (from 6.0 to 6.8 million per year). Even though the populations in southeastern South America and northeastern Brazil have decreased greatly in the last two decades relative to 1981–2000 (Supplementary Fig. 4), the population exposure to flash droughts still increased substantially or remain at a high level, highlighting the dominant roles of more intense, frequent, and widespread flash droughts in increasing the exposure of the populations in

these regions. In particular, as the world is in rapidly urbanizing, urban populations face a great threat of flash droughts, with the global average exposure of urban population to flash droughts have increased from 0.05 million per year in the period 1981–2000 to approximately 0.12 million per year during 2001–2020 (Supplementary Fig. 7). The largest increase in urban population exposure to flash droughts occurred in eastern Asia (0.26 to 0.80 million per year), followed by central Europe (0.17 to 0.46 million per year), eastern and northern America (0.33 to 0.42 million per year), southern Aisa (0.14 to 0.29 million per year), southeastern Asia (0.11 to 0.27 million per year), and Mediterranean (0.08 to 0.27 million per year). These great increases in exposure of urban populations to flash droughts highlights the urgency for targeted adaptations and early warning systems to ensure the urban water security and to improve the sustainability and livability of the world's cities.

We considered the impacts of flash droughts on agriculture, forests, and populations to generate an integrated map of exposure. The results indicated that southern Asia had the highest integrated exposure to flash droughts, mainly due to the dense population and the extensive agricultural land in this region,
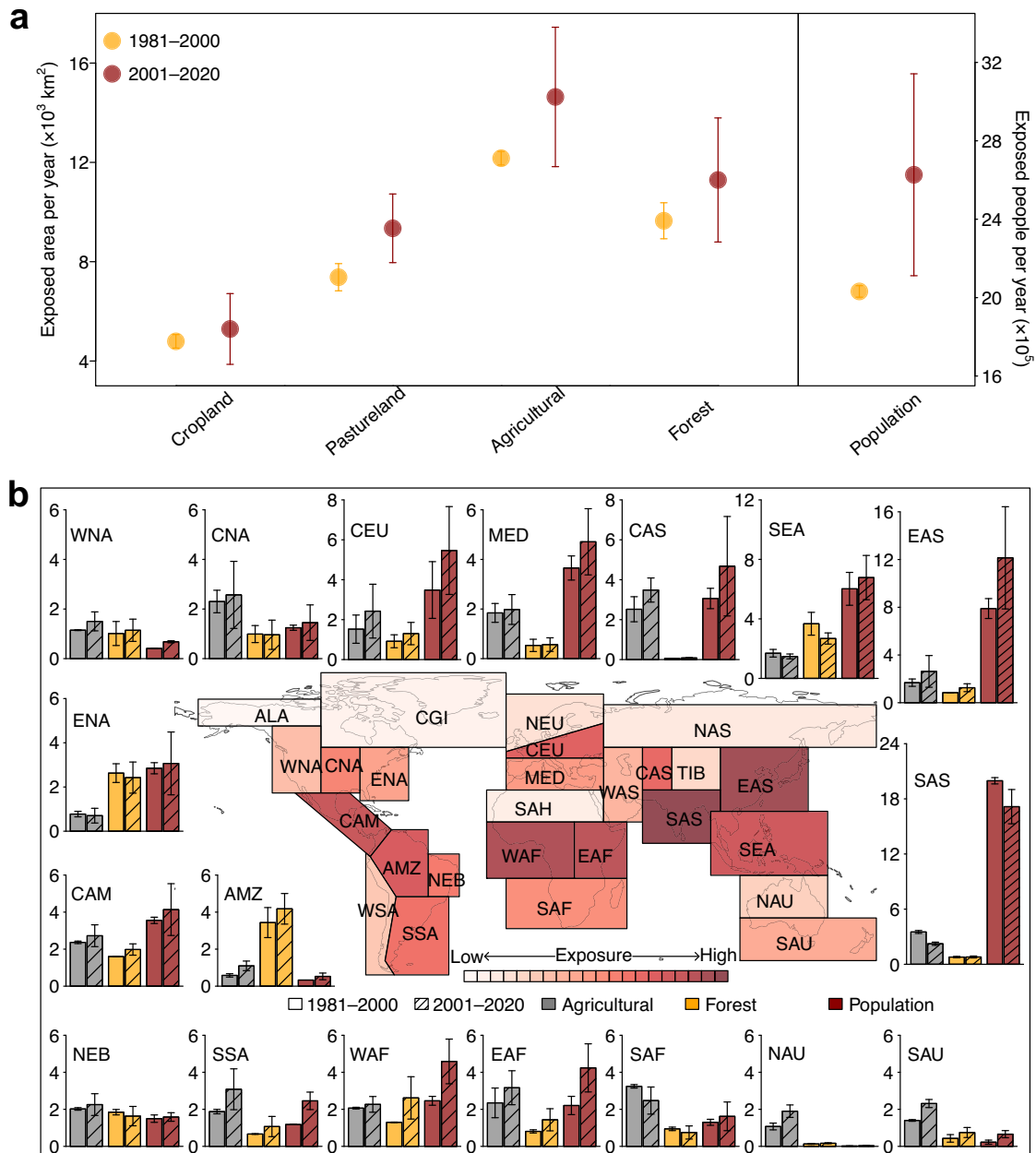
Fig. 3 Cropland, pastureland, forest, and population exposures to flash droughts. a Exposure of global mean agricultural areas (including cropland and pastureland), forested areas, and populations to flash droughts during 1981–2000 and 2001–2020. **b** Changes in mean agricultural, forest, and population exposures to flash droughts during 1981–2000 and 2001–2020 over the 26 subregions designated by recent IPCC reports. The unit for the agricultural and forest exposures is 10^4 km^2 per year, and the unit for the population exposure is 10^6 per year. The map in the center shows the spatial patterns of integrated levels of the agricultural, forest, and population exposures to flash droughts over last two decades. Error bars indicate ±1 standard error from the mean.

followed by some tropical and temperate regions, especially humid areas such as southeastern Asia, eastern Asia, northeastern Brazil, and the Amazon Basin, where exposure was lowest at high latitudes and in some extremely dry regions, such as the Sahara Desert. The low risk of formation of flash droughts at high latitudes may be due to the generally high amount of soil moisture, but in contrast, the low risk in the Sahara Desert may be because the climate is too dry to induce variations in soil moisture.

Physical drivers of flash droughts

Two key drivers were responsible for rapidly developing flash droughts: an abnormal increase in temperature and a critical lack of precipitation. When the temperature abnormally increases over an extended period of time, soil moisture can be dramatically depleted by evapotranspiration, which is strongly associated with a high VPD and solar insolation initiated by heat waves. This type of flash drought is referred to as a heat-wave flash drought. Alternatively, a persistent precipitation deficit can lead to a decrease in actual evapotranspiration and thus an increase in sensible flux under normal temperature conditions, which are responsible for (rather than caused by) the onset of heat waves and subsequently soil-moisture deficits. We refer to this type of fast-developing drought as a precipitation-deficit flash drought. Positive temperature anomalies and precipitation deficits can each promote a flash drought, and their combination can further
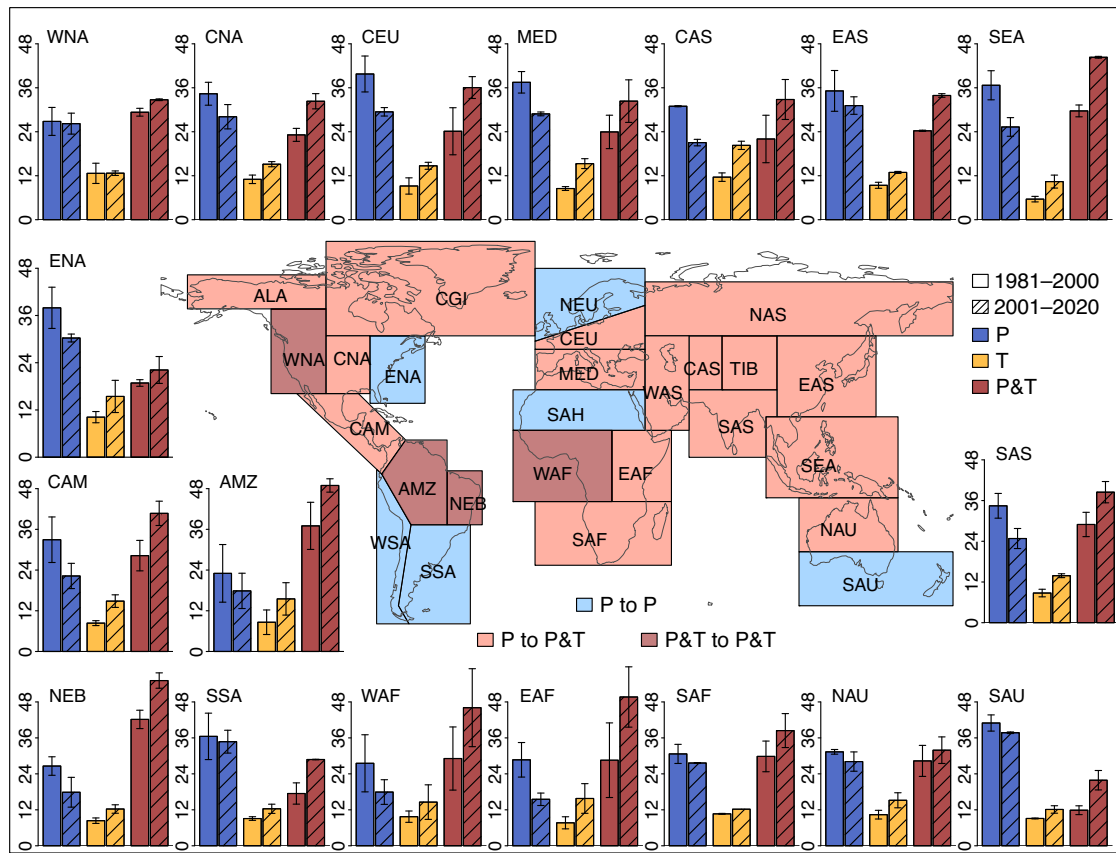
Fig. 4 Physical drivers of flash droughts during the two study periods 1981–2000 and 2001–2020. Percentage of flash droughts driven by precipitation deficits (P; i.e., precipitation-deficit flash droughts), positive temperature anomalies (T; i.e., heat-wave flash droughts), and concurrent precipitation deficits and positive temperature anomalies (P&T) during 1981–2000 and 2001–2020 calculated using two observation-based data sets over 26 subregions designated by recent IPCC reports. The mean precipitation and temperature anomalies over the time frame of the development (i.e., onset time) of flash droughts were extracted for each flash drought. P were defined as the precipitation anomaly <−0.5 and the temperature anomaly <0.5; T were defined as the precipitation anomaly >−0.5 and the temperature anomaly >0.5; P&T were defined as the precipitation anomaly <−0.5 and the temperature anomaly >0.5. The map in the center shows the dominant types of flash droughts during 1981–2000 and 2001–2020. Error bars indicate ±1 standard error from the mean.

accelerate the development of a flash drought. The relative contribution of each driver to the rapid intensification and increased frequency of flash droughts during the last two decades, however, is relatively poorly known.

We found, based on the reanalysis of global climatic data, that precipitation deficits (i.e., precipitation-deficit flash drought) accounted for 33.19% of the flash droughts globally during 1981–2000 and that flash droughts driven by abnormally high temperatures (i.e., heat-wave flash droughts) as well as concurrent precipitation deficits and positive temperature anomalies (i.e., compound hot and dry flash droughts) accounted for only 9.89% and 24.5%, respectively, of the flash droughts (Supplementary Fig. 8). The global mean percentage of compound hot and dry flash droughts increased to 34.13% and heat-wave flash droughts increased to 15.3% in the last two decades, whereas the percentage of precipitation-deficit flash droughts decreased to 26.0%. These findings indicate that climate change in the last few decades has driven a shift from a period dominated by precipitation-deficit flash droughts to a period characterized by more heat-wave and concurrent hot and dry flash droughts.

The dominant drivers of flash droughts, however, varied regionally around the globe (Fig. 4). Flash droughts in Amazon Basin, northeastern Brazil, western Africa, and northwestern America were primarily driven by concurrent precipitation deficits and positive temperature anomalies during both the periods 1981–2000 and 2001–2020. The percentages of these compound hot and dry flash droughts increased from 37.0%, 42.2%, 29.1%,

and 29.3% during 1981–2000 to 48.9%, 55.1%, 46.1%, and 32.7% during 2001–2020 in Amazon Basin, northeastern Brazil, western Africa, and northwestern America, respectively (Fig. 4). Sahara Desert, southern Australia, southeastern and west-coast South America, northeastern America, and northern Europe were the only six regions where the primary driver of flash droughts were precipitation deficits during both the periods 1981–2000 and 2001–2020. In all other regions, the primary driver of flash droughts has shifted from precipitation deficits during 1981–2000 to concurrent precipitation deficits and positive temperature anomalies in the last two decades. These results collectively indicated that the increase in concurrent extremely low precipitation and high temperatures under global warming was the main driver of the recent higher frequency and faster developing flash droughts.

CMIP6 models underestimated the occurrence of flash droughts

On the basis of the aforementioned findings, we evaluated the performance of 22 Earth system models in CMIP6 in reproducing the characteristics and main drivers of flash droughts by using their outputs for daily soil moisture, precipitation, and temperature (Fig. 5). The results indicated that the CMIP6 models could simulate well the geographical distribution of areas prone to flash droughts during the two study periods, with foci mainly in the Amazon Basin, southeastern North America, northern Europe,
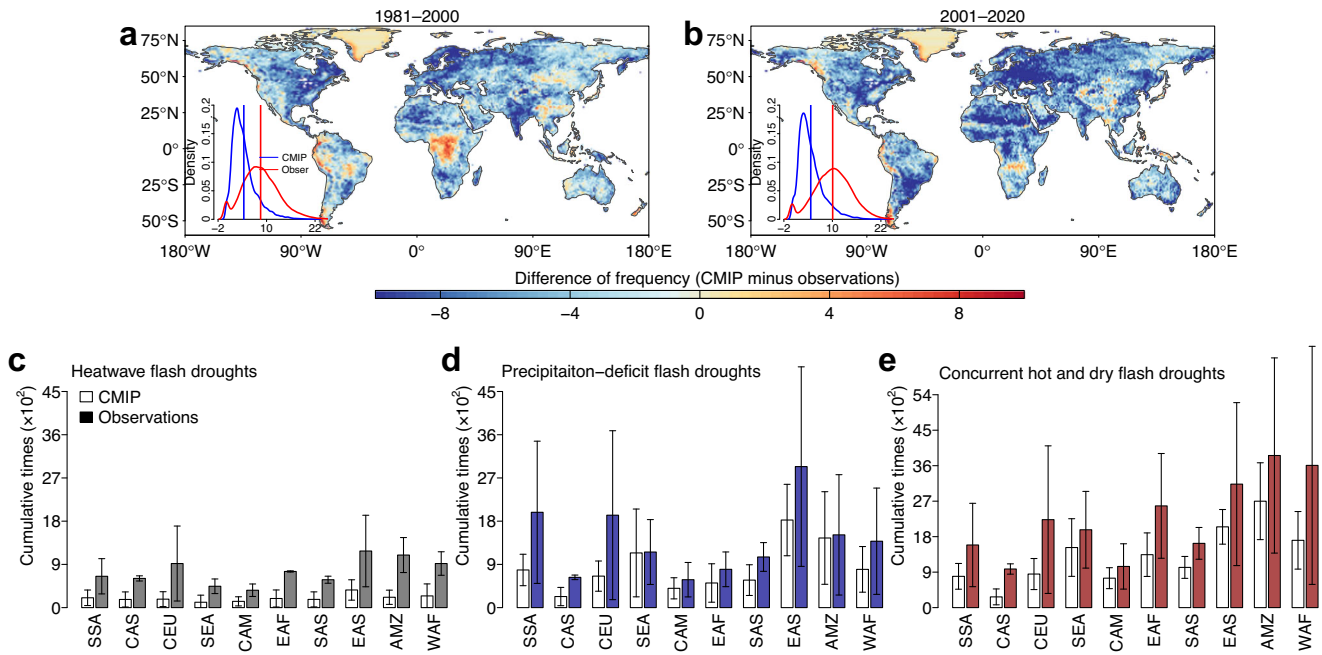
Fig. 5 Characteristics and drivers of flash droughts calculated according to 22 CMIP6 models. Spatial patterns of the difference in the frequency of flash droughts between the frequency calculated using two observation-based data sets and frequency calculated using the CMIP6 models for **a** 1981–2000 and **b** 2001–2020 (CMIP minus observations). The insets represent the probability distribution of drought frequency calculated using observation-based data sets (red line) and CMIP6 models (blue line). Accumulated occurrences of flash droughts driven by **c** precipitation deficits, **d** positive temperature anomalies, and **e** concurrent precipitation deficits and positive temperature anomalies over the last two decades calculated using two observation-based data sets and the CMIP6 outputs. Error bars indicate ±1 standard error from multi-model means.

central Africa, and southeastern Asia. The frequency of flash droughts also reflected a widespread increase in the last two decades relative to 1981–2000 (Supplementary Fig. 9). The CMIP6 models, however, were unable to simulate the increasing trends of flash droughts that developed within one and two pentads and those that developed into long-term seasonal droughts (Supplementary Fig. 10). In particular, compared with the observation-based (i.e., Global Land Evaporation Amsterdam Model [GLEAM] and ECMWF Reanalysis v5 [ERA5]) results, the CMIP6 simulations greatly underestimated the frequency of flash droughts over approximately 85.1 and 89.6% of the global land surface during 1981–2000 and 2001–2020, respectively, especially in temperate regions (Fig. 5).

In terms of physical drivers, the CMIP6-simulated results also indicated that most flash droughts were primarily driven by concurrent precipitation deficits and positive temperature anomalies during the last two decades and that the accumulated occurrences of compound hot and dry flash droughts were comparable to or even slightly larger than the observation-based occurrences in some subregions (Fig. 5e, Supplementary Fig. 11). This may be related to the fact that CMIP6 models have extensively overestimated the dependence between extremely low precipitation and high temperatures at short timescales (e.g., 5 days), especially for some dry regions, such as Sahara Desert and northern Australia (Supplementary Fig. 12). But for most temperate and high latitudes of northern Hemisphere, the accumulated occurrences of compound hot and dry flash droughts and the dependence between extremely low precipitation and high temperatures simulated by the CMIP6 models were greatly lower than observation-based results. Similarly, the accumulated occurrences of precipitation-deficit flash droughts, especially the heat-wave flash droughts simulated by the CMIP6 models were much lower than the observation-based occurrences in all subregions (Fig. 5c, d; Supplementary Fig. 11). This suggests that CMIP6 models may have also underestimated the individual

effects of precipitation deficits and heat waves in promoting flash droughts because they underestimate the sensitivity of soil moisture to temperature and precipitation at short timescales (e.g., 5 days; Supplementary Fig. 13).

DISCUSSION

This study provides a comprehensive understanding of the characteristics, mechanisms, and impacts of changes to flash droughts in the last four decades. Our results indicate that flash droughts increased considerably after 2000, mainly because of the widespread increase in the co-occurrence of extremely hot and dry conditions in a warming climate (Fig. 4). The warmer temperature can naturally increase these compound extremes by greatly increasing the atmospheric water demand, which can induce dry conditions even if precipitation does not change or even increases slightly[35,36]. These findings are consistent with those of Yuan et al.[16], who reported that anthropogenic warming induced by increased concentrations of greenhouse gases has increased the variability of precipitation and temperature by increasing evapotranspiration, accounting for 77 ± 26% of the upward trend in flash droughts. In addition to the warming trend, our results indicated that a strengthening of the dependence between temperature and precipitation further exacerbated the increase in concurrent hot and dry conditions at a short timescale (e.g., 5 days) in many regions (Supplementary Fig. 12), suggesting that even if systems were to adapt to the mean climate change, they would be subjected to concurrent hot and dry conditions and thus experience flash droughts more frequently. In particular, anthropogenic warming will likely continue for a long time, and the co-occurrence of extremely hot and dry conditions is projected to increase[37,38], both of which will lead to more prevalent flash droughts in the future.

In addition to the increasing trend, flash droughts are characterized by an accelerated onset and longer duration

(Fig. 2). These may be mostly attributed to the self-intensification and self-propagation of drought under the strengthened land–atmosphere feedbacks and large-scale atmospheric dynamics[15,39,40]. Specifically, the depletion of soil moisture induced by negative precipitation anomalies could lead to a decrease in evapotranspiration, leading to higher temperatures and VPDs resulting from increased sensible heat flux and reduced near-surface humidity. A higher VPD, however, can in turn increase the atmospheric evaporative demand and further accelerate the depletion of soil moisture. These land–atmospheric feedbacks are strengthened under global warming and can induce the co-occurrence of anomalies in multiple factors (e.g., VPD, temperature, and precipitation)[38], which may thus trigger and accelerate the onset of flash droughts. Most important, from a Lagrangian perspective, is that land–atmospheric feedbacks may also prolong the life expectancy of flash droughts by aiding them in extending to other locations, or even triggering new events in remote teleconnected regions[38,39,41]. For example, if a flash drought occurs in a region where moisture is highly recycled (i.e., where local precipitation is mostly due to local evaporation), the reduced precipitation during a flash drought can persistently dry the soil and subsequently reduce evaporation, which in turn further reduces the likelihood of rain and thus induces the self-intensification of a local drought. Alternatively, if a flash drought occurs in an upwind region (source), where terrestrial evaporation contributes a substantial amount of moisture for precipitation to downwind (sink) regions, the heat and deficit of atmospheric moisture during the drought can thus propagate from the upwind region to the downwind regions[42], leading to the expansion of flash droughts into neighboring areas or even concurrently into a series of events, thus inducing the self-propagation of flash droughts, especially for drylands[39]. This strengthened self-intensification and self-propagation of droughts in a warming climate may mostly account for why flash droughts tend to be longer or even transform into long-term seasonal droughts. However, the concept of teleconnected land–atmosphere feedbacks is still new; thus, clarifying the processes of water vapor and heat transport across land surfaces during droughts may contribute to our understanding of the development of flash droughts and the link between flash droughts and conventional long-term seasonal droughts.

Forests exposed to a comparable increase in flash droughts to that of agriculture (Fig. 3), which may have a large impact on ecosystem services, because protecting forests may be the most effective natural solution that can substantially contribute to the mitigation of climate change[43]. Vegetation productivity has increased substantially in the last three decades because of the increase in atmospheric levels of carbon dioxide (CO_2) and the subsequent stimulation of photosynthetic activity[44,45], providing a net carbon sink for approximately 30% of the CO_2 emitted by industry and the burning of fossil fuels[46], with the majority estimated to occur in forests[47]. The continuous increase in flash droughts, during which the co-occurrence of extremely high VPDs and temperatures and low levels of soil moisture, however, can jointly inhibit plant growth or even lead to plant mortality, which may further accelerate global warming by releasing more carbon to the atmosphere or may even transform terrestrial ecosystems from carbon sinks to carbon sources, especially for the Amazon and Congo Basins (Fig. 2). Changes in the status of vegetation growth can in turn also affect the development of flash droughts. The warming temperature has widely advanced the spring emergence of leaves[48–50], which, combined with the stimulation of vegetation growth by favorable climatic conditions (e.g., temperature, solar radiation, and increasing CO_2 concentrations) in the early stages of growth, may induce additional deficits of soil moisture in late spring by increasing evapotranspiration[51–53]. These deficits of soil moisture may persist or even extend into the following summer by further increasing the temperature and thus

induce the development of flash droughts. These possibilities may partially account for why most flash droughts tended to occur in vegetated areas and were concentrated in late spring and early summer (Fig. 2). In particular, flash droughts that develop under these conditions generally indicate that the stimulation of vegetation growth in the early growing season exceeded the carrying capacities of the ecosystems (i.e., structural overshoot) such that the ecosystems became more susceptible to such structural overshoot flash droughts[54]. The contribution of increased water consumption by vegetation to the development and evolution of flash droughts, however, remains unappreciated; a precise quantification of the atmosphere–biosphere interaction is thus needed to better predict the impacts of flash droughts in a changing climate.

The CMIP6 models provide a unique opportunity to forecast disasters and early warnings and thus have been widely used to project and identify changes in the characteristics of flash droughts[55,56]. When analyzed using CMIP6 models, our results were generally consistent with Yuan et al.[29], who suggested that amplified anomalies of evapotranspiration and precipitation deficit driven by anthropogenic climate change has sped up drought onset and are expected to accelerate the global transition to more frequent flash droughts on a global scale under the higher-emission scenario. However, our findings also indicate that the CMIP6 models greatly underestimated the frequency of flash droughts in most study regions, especially flash droughts driven by heat waves (Fig. 5), suggesting that extremely high temperatures alone could not lead to a decrease in soil moisture in the CMIP6 models. This may be because the CMIP6 models do not effectively simulate available root-zone soil moisture for evapotranspiration but instead rely excessively on the storage of water in shallow soil and water intercepted by canopies, which strongly depend on precipitation, to supply evapotranspiration[57,58]. Lower precipitation can thus lead to a negative evapotranspiration bias in the CMIP6 models and a corresponding positive temperature bias by increasing the sensible flux from land–atmospheric feedbacks, causing a net overestimation of the dependence between low precipitation and high temperature at short time-scales, especially for dry regions (e.g., 5 days; Supplementary Fig. 12). In particular, the low sensitivity of soil moisture to extremely high temperatures in the CMIP6 models may lead to a larger underestimation of the occurrences and onset times of flash droughts in the future (Supplementary Fig. 13), when heat waves will become more common and the higher atmospheric water demand induced by warming is expected to play a more important role in the formation of flash droughts[59,60]. We thus emphasize that future occurrences of flash droughts are likely to be more severe than those projected based on soil moisture in CMIP6 models and that hydrological-cycle bias associated with warming (e.g., errors in transpiration–evaporation partitioning) should be revised in the CMIP6 models to potentially serve as a reliable early-warning tool for flash droughts.

In summary, our study provides a comprehensive analysis of the characteristics, driving mechanisms, and associated impacts of flash droughts at site and global scales based on FLUXNET, global reanalysis, and CMIP6 data sets. Results indicated that flash droughts not only increased significantly in frequency in the last two decades, but also tended to be more "flash" and to last longer, which was mostly attributed to the increased concurrent hot and dry extremes at a short timescale (5 days) in a warming climate. These changes have increased the exposures of agricultural areas, forested areas, and populations to flash droughts by 20.3%, 17.1%, and 30.0%, respectively, during 2001–2020 compared to 1981–2000, with the regions of highly integrated exposure mainly in vegetated and densely populated areas. The CMIP6 models slightly overestimated the occurrence of flash droughts driven by concurrent hot and dry conditions in some dry regions but nearly globally underestimated the frequency of flash droughts driven by

either precipitation deficits or heat waves. These over- and underestimations may have been due to the misrepresentation by the CMIP6 models of the dependence between extremely low precipitation and high temperatures at short timescales and to the underestimation of their individual effects in promoting flash droughts. Our results highlight that the hydrological-cycle bias associated with warming at short timescales (e.g., 5 days) may need to be revised in the CMIP6 models to provide more reliable projections of flash droughts.

METHODS

FLUXNET data

We primarily used data for daily soil moisture, temperature, and precipitation from the FLUXNET2015 dataset to examine the characteristics of flash droughts at the site scale. Soil moisture was measured as volumetric water concentration (percentage) in surface soil (varying across sites but mainly at depths of 5–10 cm) because moisture in deep soil were measured at only a limited number of sites. We ultimately selected 36 sites (473 site-years) with data covering no fewer than 10 years ranging from 1996 to 2014. These FLUXNET observations included data from three grassland sites, six cropland sites, seven sites in deciduous broadleaf forests, and 11 sites in evergreen needleleaf forests. Detailed information for the sites is listed in Supplementary Table 1. All data for daily soil moisture, temperature, and precipitation were aggregated on a pentad (5-day) timescale to extract the flash droughts and were then analyzed to identify changes and key drivers. The total number of flash droughts for each year was first normalized by using the number of stations with data coverage in that year (i.e., the number of flash droughts divided by the number of sites with data coverage in that year) to indicate the general temporal trend of flash droughts over all stations because of the different time ranges of data from different sites.

Data for soil moisture

We used two global data sets of root-zone soil moisture from the GLEAM and ECMWF Reanalysis v5 (ERA5; upper 100 cm of soil) to identify spatial and temporal changes in the characteristics of flash droughts during 1981–2020 at a global scale. The GLEAM Soil Moisture V3.5a data are available on a 0.25° × 0.25° latitude/longitude grid with daily temporal resolution for 1980–2020. These data have been extensively validated as being highly consistent with soil moisture measured from eddy-covariance towers and soil-moisture sensors across a broad range of ecosystems[61]. The ERA5 soil moisture data is available at a high spatial resolution of 0.25° × 0.25° and four layers (i.e., 0–7 cm, 7–28 cm, 28–100 cm, and 100–289 cm) for the period 1950 to near real-time[62]. Recent studies have suggested that the reasonable skill of ERA5 soil moisture simulation compared to observations across different locations[63]. The top-1m ERA5 soil moisture data were used in our study to extract flash drought events. All these soil moisture data were aggregated to daily and 1° × 1° latitude/longitude grids.

CMIP6 data

The data for daily precipitation, temperature, and soil moisture from CMIP6 simulations produced by 22 Earth system models covering historical (1981–2014) and future (2015–2020 under a high-emissions scenario, SSP5-8.5) periods were used to assess the performance of CMIP6 models in reproducing the characteristics of flash droughts relative to the observation-based results (i.e., results generated by using the GLEAM and ERA5 datasets). It should be noted that the daily precipitation, temperature, and soil moisture data are available from a total of 22 CMIP6 models published by 11 institutes under historical and SSP5-8.5 scenarios

with the variant label of "r1i1p1f1" and "r1i1p1f2", so far. All these models are included in our analysis and the details are presented in Supplementary Table 2. The CMIP6 model data were bilinearly interpolated to a spatial resolution of 1° × 1° to match the GLEAM and ERA5 data.

Other data sets

Daily precipitation and temperature data from ERA5 were also used to analyze the contributions of precipitation deficits and positive temperature anomalies to the occurrence of flash droughts. In addition, we obtained population data from 2000 and 2020 at spatial resolutions of 1 km from Gao[64] and obtained the fractions of cropland and pastureland for 2000 at spatial resolutions of 10 km) from the NASA Socioeconomic Data and Applications Center[65] to calculate the changes in agricultural (including cropland and pastureland) and population exposures. To specifically asses the urban population exposure, we also obtained the urban extents data from 2000 and 2020 at spatial resolutions of 0.0083° × 0.0083° grids from Zhao et al.[66]. To assess the forest exposure, we inferred global tree-cover data for 2009 at a spatial resolution of 1 arc-s from the global forest change version 1.6 dataset, where tree cover was defined as the areal coverage of canopies higher than 5 m[67]. Population size varied spatially and depended on regional interactions[68]. The traditional methods of interpolation were thus not suitable for scaling up the population data to match the 1° × 1° grid scale. We therefore aggregated the population data across the grid cells (at a spatial resolution of 1 km) within the 1° × 1° grid cells to calculate population exposure. The same operation was performed for urban extents, cropland, and pastureland and for the tree-cover data.

Analysis of the characteristics of flash droughts

After identifying all flash droughts according to our definition (Fig. 1a), we defined the frequency of flash droughts as the number of occurrences during a specific period. To investigate the temporal changes of flash droughts regionally or globally, we calculated the yearly accumulated flash-drought occurrences (AFDs):

$$AFDs = \sum_{j=1}^{Nj} \sum_{i=1}^{Ni} FDs \times A(i,j), \qquad (1)$$

where FDs is the frequency of flash droughts and $A(i,j)$ is the area weight for the pixel at longitude i and latitude j for a specific region. The increase in AFDs indicates an increase in the frequency of flash droughts or in the area affected by flash droughts, or both. The AFDs were also calculated by using timescales of the starting month, duration, and onset development to comprehensively analyze the changes in other characteristics of flash droughts.

Precipitation and temperature are the two main drivers of flash droughts[9,10]. We analyzed the contributions of precipitation deficits, positive temperature anomalies, and their combined effects to the development of flash droughts by first aggregating the data for daily precipitation and temperature (tem) to a pentad (5-day) timescale and then calculating their standardized anomalies:

$$SA_{tem} = \frac{tem^{x,y} - \overline{tem^{x,y}}}{\sigma(tem^{x,y})}, \qquad (2)$$

where SA_{tem} is the standardized anomaly sequences of temperature, $tem^{x,y}$ is the temperature at grid x for pentad y of the year during the reference period (1981–2020), $\overline{tem^{x,y}}$ is the mean of $tem^{x,y}$, and $\sigma(tem^{x,y})$ is the standard deviation of $tem^{x,y}$. The standardized anomalies of 5-day aggregated precipitation were calculated in the same way.

The mean precipitation and temperature anomalies over the onset time (t_0–t_1 in Fig. 1a) of flash droughts were extracted for each flash drought. If the precipitation anomaly was less than

–0.5 and the temperature anomaly was less than 0.5, the flash drought was primarily driven by a precipitation deficit (i.e., a precipitation-deficit flash drought). If the precipitation anomaly was greater than –0.5 and the temperature anomaly was greater than 0.5, the flash drought was mainly driven by abnormally high temperatures (i.e., a heat-wave flash drought). If the precipitation anomaly was less than –0.5 and the temperature anomaly was greater than 0.5, the flash drought was driven by a concurrent precipitation deficit and positive temperature anomaly (i.e., a concurrent hot and dry flash drought). The threshold of 0.5 (precipitation or temperature anomalies accounted for nearly 70% of the flash droughts) was set based on the trade-off between stringency and interpretability. If the threshold was set to 1, the precipitation or temperature could account for only approximately 30% of the flash droughts, which was too strict for a universal attribution.

Calculation of agriculture, forest, and population exposures

Given the importance of pastureland for grazing animals, cropland for producing food, and forests for storing carbon, we quantified the risk of exposure of these land types to flash droughts regionally or globally:

$$\text{Cropland, pastureland, and forest exposures}: \frac{1}{Y}\sum_{y=1}^{Y}\sum_{j=1}^{Nj}\sum_{i=1}^{Ni}\text{Ps}\times a(i,j), \quad (3)$$

where Y is number of years for a specific period, y is the year with flash droughts, Ps is the number of pentads under flash droughts for year y, and $a(i,j)$ is the total area of cropland, pastureland, or forest affected by drought for the pixel at longitude i and latitude j. Cropland and pastureland data were based on data from 2000, and tree cover was based on data from 2009 and was fixed for both study periods, 1981–2000 and 2001–2020. We also similarly calculated the population exposures to indicate the impacts of flash droughts on human society:

$$\text{Population exposures}: \frac{1}{Y}\sum_{y=1}^{Y}\sum_{j=1}^{Nj}\sum_{i=1}^{Ni}\text{Ps}\times\text{Peos}(i,j), \quad (4)$$

In the same way, the urban population exposure to flash droughts can be calculated as:

$$\text{Urban population exposures}: \frac{1}{Y}\sum_{y=1}^{Y}\sum_{j=1}^{Nj}\sum_{i=1}^{Ni}\text{Ps}\times\text{Peos}(i,j)\times\text{Perc}(i,j), \quad (5)$$

where Peos is the number of people and Perc is the percentage of urban extents for the pixel affected by drought at longitude i and latitude j. The population and urban extents data for 1981–2000 were based on data from 2000, and the population and urban extents data for 2001–2020 were based on data from 2020.

The agricultural (including cropland and pastureland), forest, and population exposures were first regionally normalized to produce an integrated exposure map of 26 wide geographical regions designated in a recent IPCC report[34]. Using population exposure as an example:

$$\text{Regionally normalized population exposures}: \frac{E_i - E_{\max}}{E_{\max} - E_{\min}}, \quad (6)$$

where E_i is the population exposure for region i, and $E_{\max}$ and $E_{\min}$ are the maximum and minimum population exposures over 26 regions, respectively. The means of regionally normalized agricultural, forest, and population exposures for a region indicate the level of composite exposure.

Investigation of the dependence between low precipitation and high temperature

The dependence between 5-day mean precipitation and temperature in our study was formulated by using (1) Pearson's

correlations and (2) bivariate copulas[69], which have been extensively used as an effective statistical method to describe the dependence between random variables and to derive the joint probability of a compound extreme[38,70]. Assuming two random variables, A (e.g., precipitation) and B (e.g., temperature), with marginal cumulative distribution functions $F_A(a) = P_r(A \leq a)$ and $F_B(b) = P_r(B \leq b)$, respectively, their joint probability distribution can be obtained by the copula (C):

$$F(a,b) = P_r(A \leq a, B \leq b) = C[F_A(a), F_B(b)], \quad (7)$$

where $F(a,b)$ is the joint distribution function of A and B. The two marginal distribution functions $F_A(a) = P_r(A \leq a)$ and $F_B(b) = P_r(B \leq b)$ were converted into two uniformly distributed random variables W and Z that ranged from 0 to 1, so the joint probability distribution of A and B can be described as

$$F(a,b) = C(W,Z), 0 \leq W, Z \leq 1, \quad (8)$$

The probability of an extreme compound event, in which the variables were below or above a given threshold, is thus expressed as

$$p = P_r(W > w \cap Z \leq z) = z - C(w,z), \quad (9)$$

The concurrent hot (i.e., high temperature) and dry (i.e., low precipitation) conditions in our study were defined as 5-day mean precipitation below its 10th percentile and 5-day mean temperature above its 90th percentile, and the probability of such a co-occurrence extreme can thus be calculated as

$$p = P_r(W > 0.9 \cap Z \leq 0.1) = 0.1 - C(0.9, 0.1), \quad (10)$$

We obtained the uniform distributions of 5-day mean precipitation and temperature by first converting their marginal distributions to a normalized rank that ranged from 0 to 1, which is a general operation when using copulas[37]. We then fitted all possible families of bivariate copulas (a total of 39, listed in Supplementary Table 3) and chose the copula with the best fit in each pixel by using the Bayesian Information Criterion implemented in the VineCopula R package[71]. We used the best fitting copula to calculate the probability of occurrence of compound low-precipitation and high-temperature extremes by using Eq. 9 and the "BiCopCDF" function in VineCopula. In addition, we also calculated the probability of occurrence of compound low-precipitation and high-temperature extremes by each of four widely used copula functions (i.e., Gaussian, Clayton, Gumble, and Frank copulas) globally, and the results were highly consistent (Supplementary Fig. 14). This indicated that the assignation of different copulas in different pixels has little effects on our main results.

If the 5-day mean precipitation and temperature were independent, the probability of a concurrent hot (i.e., temperature above its 90th percentile) and dry (precipitation below its 10th percentile) extreme would be $0.1 \times 0.1 = 0.01$. We therefore defined the likelihood multiplication factor (LMF) as the ratio of the joint probability calculated by the copula to that assuming they were independent (i.e., 0.01) to measure the strength of dependence of bivariate extremes, and an LMF of 1 thus represents no increase in the cooccurrence probability.

Investigation of the sensitivity of soil moisture to precipitation and temperature

The sensitivity of 5-day mean soil moisture to precipitation and temperature were analyzed by partial correlation, which measures the individual effect of a parameter on the variance of the predicted values when the effect of the other parameters has been eliminated. The details were formulated by the following

equation[72]:

$$R_{xy,z} = \frac{R_{xy} - R_{xz}R_{yz}}{\sqrt{\left(1 - R_{xz}^2\right)\left(1 - R_{yz}^2\right)}},$$ (11)

where $R_{xy,z}$ is the correlation between parts x (e.g., soil moisture) and y (e.g., precipitation) while controlling for the possible influences of z (e.g., temperature). The larger the partial correlation coefficient between x and y (e.g., $R_{xy,z}$), the more sensitive x is to y.

To better characterize the CMIP model results, the correlation, LMF, and partial correlation were fist calculated for each individual CMIP6 model; then, the ensemble-mean correlation coefficients, LMFs, and partial correlation coefficients were compared with those calculated using observation-based data sets.

DATA AVAILABILITY
The data that support the findings of this study are publicly available from the following resources. The FLUXNET2015 dataset is available at http://fluxnet.fluxdata.org/data/fluxnet2015-dataset/. The GLEAM soil-moisture data set is available at http://www.gleam.eu/. The ERA5 soil moisture, precipitation, and temperature data are available at https://www.ecmwf.int/en/forecasts/dataset/ecmwf-reanalysis-v5. The CMIP6 data sets are available at https://esgf-node.llnl.gov/projects/cmip6/. The population and agricultural land data sets are publicly available at the NASA Socioeconomic Data and Applications Center (https://sedac.ciesin.columbia.edu). The urban extents data are available at https://doi.org/10.6084/m9.figshare.16602224.v1. The forest-cover data are available at https://earthenginepartners.appspot.com/science-2013-global-forest/download_v1.4.html.

CODE AVAILABILITY
Analysis and figure generation were performed using R and Python, and the codes are available from the corresponding author.

REFERENCES
1. Overpeck, J. T. The challenge of hot drought. *Nature* **503**, 350–351 (2013).
2. Brodribb, T. J., Powers, J., Cochard, H. & Choat, B. Hanging by a thread? Forests and drought. *Science* **368**, 261–266 (2020).
3. Naumann, G., Cammalleri, C., Mentaschi, L. & Feyen, L. Increased economic drought impacts in Europe with anthropogenic warming. *Nat. Clim. Change* **11**, 485–491 (2021).
4. Ault, T. R. On the essentials of drought in a changing climate. *Science* **368**, 256–260 (2020).
5. Trenberth, K. E. et al. Global warming and changes in drought. *Nat. Clim. Change* **4**, 17–22 (2014).
6. Sheffield, J., Wood, E. F. & Roderick, M. L. Little change in global drought over the past 60 years. *Nature* **491**, 435–438 (2012).
7. Parker, T., Gallant, A., Hobbins, M. & Hoffmann, D. Flash drought in Australia and its relationship to evaporative demand. *Environ. Res. Lett.* **16**, 064033 (2021).
8. Pendergrass, A. G. et al. Flash droughts present a new challenge for subseasonal-to-seasonal prediction. *Nat. Clim. Change* **10**, 191–199 (2020).
9. Mo, K. C. & Lettenmaier, D. P. Heat wave flash droughts in decline. *Geophys. Res. Lett.* **42**, 2823–2829 (2015).
10. Mo, K. C. & Lettenmaier, D. P. Precipitation deficit flash droughts over the United States. *J. Hydrometeorol.* **17**, 1169–1184 (2016).
11. Otkin, J. A. et al. Flash droughts: a review and assessment of the challenges imposed by rapid-onset droughts in the United States. *Bull. Am. Meteorol. Soc.* **99**, 911–919 (2018).
12. Lisonbee, J., Woloszyn, M. & Skumanich, M. Making sense of flash drought: Definitions, indicators, and where we go from here. *J. Appl. Meteorol. Climatol.* **2021**, 1–19 (2021).
13. Hoerling, M. et al. Causes and predictability of the 2012 Great Plains drought. *Bull. Am. Meteorol. Soc.* **95**, 269–282 (2014).
14. Nguyen, H., Wheeler, M. C., Otkin, J. A., Cowan, T., Frost, A. & Stone, R. Using the evaporative stress index to monitor flash drought in Australia. *Environ. Res. Lett.* **14**, 064016 (2019).
15. Qing, Y., Wang, S., Ancell, B. C. & Yang, Z.-L. Accelerating flash droughts induced by the joint influence of soil moisture depletion and atmospheric aridity. *Nat. Commun.* **13**, 1139 (2022).
16. Yuan, X., Wang, L., Wu, P., Ji, P., Sheffield, J. & Zhang, M. Anthropogenic shift towards higher risk of flash drought over China. *Nat. Commun.* **10**, 4661 (2019).
17. Basara, J. B., Christian, J. I., Wakefield, R. A., Otkin, J. A., Hunt, E. H. & Brown, D. P. The evolution, propagation, and spread of flash drought in the Central United States during 2012. *Environ. Res. Lett.* **14**, 084025 (2019).
18. Anderson, M. C. et al. The Evaporative Stress Index as an indicator of agricultural drought in Brazil: An assessment based on crop yield impacts. *Remote Sens. Environ.* **174**, 82–99 (2016).
19. Christian, J. I. et al. Global distribution, trends, and drivers of flash drought occurrence. *Nat. Commun.* **12**, 6330 (2021).
20. Otkin, J. A., Anderson, M. C., Hain, C. & Svoboda, M. Examining the relationship between drought development and rapid changes in the evaporative stress index. *J. Hydrometeorol.* **15**, 938–956 (2014).
21. Hobbins, M. T. et al. The evaporative demand drought index. Part I: Linking drought evolution to variations in evaporative demand. *J. Hydrometeorol.* **17**, 1745–1761 (2016).
22. Noguera, I., Domínguez-Castro, F. & Vicente-Serrano, S. M. Characteristics and trends of flash droughts in Spain, 1961-2018. *Ann. N.Y. Acad. Sci.* **1472**, 155–172 (2020).
23. Hunt, E. D., Svoboda, M., Wardlow, B., Hubbard, K., Hayes, M. & Arkebauer, T. Monitoring the effects of rapid onset of drought on non-irrigated maize with agronomic data and climate-based drought indices. *Agric. Meteorol.* **191**, 1–11 (2014).
24. Mohammadi, K., Jiang, Y. & Wang, G. Flash drought early warning based on the trajectory of solar-induced chlorophyll fluorescence. *Proc. Natl Acad. Sci.* **119**, e2202767119 (2022).
25. Osman, M. et al. Flash drought onset over the contiguous United States: sensitivity of inventories and trends to quantitative definitions. *Hydrol. Earth Syst. Sci.* **25**, 565–581 (2021).
26. Zhang, M. & Yuan, X. Rapid reduction in ecosystem productivity caused by flash droughts based on decade-long FLUXNET observations. *Hydrol. Earth Syst. Sci.* **24**, 5579–5593 (2020).
27. Koster, R., Schubert, S., Wang, H., Mahanama, S. & DeAngelis, A. M. Flash drought as captured by reanalysis data: Disentangling the contributions of precipitation deficit and excess evapotranspiration. *J. Hydrometeorol.* **20**, 1241–1258 (2019).
28. Mukherjee, S. & Mishra, A. K. A multivariate flash drought indicator for identifying global hotspots and associated climate controls. *Geophys. Res. Lett.* **49**, e2021GL096804 (2022).
29. Yuan, X., Wang, Y., Ji, P., Wu, P., Sheffield, J. & Otkin, J. A. A global transition to flash droughts under climate change. *Science* **380**, 187–191 (2023).
30. Yuan, W. et al. Increased atmospheric vapor pressure deficit reduces global vegetation growth. *Sci. Adv.* **5**, eaax1396 (2019).
31. Perkins-Kirkpatrick, S. & Lewis, S. Increasing trends in regional heatwaves. *Nat. Commun.* **11**, 3357 (2020).
32. Williams, A. P. et al. Large contribution from anthropogenic warming to an emerging North American megadrought. *Science* **368**, 314–318 (2020).
33. Ford, T. W. & Labosier, C. F. Meteorological conditions associated with the onset of flash drought in the eastern United States. *Agric. Meteorol.* **247**, 414–423 (2017).
34. Field, C. B., Barros, V., Stocker, T. F. & Dahe Q. *Managing the Risks of Extreme Events and Disasters to Advance Climate Change Adaptation: Special Report of the Intergovernmental Panel on Climate Change.* Cambridge University Press (2012).
35. Alizadeh, M. R., Adamowski, J., Nikoo, M. R., AghaKouchak, A., Dennison, P. & Sadegh, M. A century of observations reveals increasing likelihood of continental-scale compound dry-hot extremes. *Sci. Adv.* **6**, eaaz4571 (2020).
36. Hao, Z., AghaKouchak, A. & Phillips, T. J. Changes in concurrent monthly precipitation and temperature extremes. *Environ. Res. Lett.* **8**, 034014 (2013).
37. Zscheischler, J. & Seneviratne, S. I. Dependence of drivers affects risks associated with compound events. *Sci. Adv.* **3**, e1700263 (2017).
38. Zhou, S. et al. Land–atmosphere feedbacks exacerbate concurrent soil drought and atmospheric aridity. *Proc. Natl Acad. Sci.* **116**, 18848–18853 (2019).
39. Schumacher, D. L., Keune, J., Dirmeyer, P. & Miralles, D. G. Drought self-propagation in drylands due to land–atmosphere feedbacks. *Nat. Geosci.* **15**, 262–268 (2022).
40. Wang, Y. & Yuan, X. Land-atmosphere coupling speeds up flash drought onset. *Sci. Total Environ.* **851**, 158109 (2022).
41. Schumacher, D. L., Keune, J., Van Heerwaarden, C. C., Vilà-Guerau de Arellano, J., Teuling, A. J. & Miralles, D. G. Amplification of mega-heatwaves through heat torrents fuelled by upwind drought. *Nat. Geosci.* **12**, 712–717 (2019).
42. Herrera-Estrada, J. E., Martinez, J. A., Dominguez, F., Findell, K. L., Wood, E. F. & Sheffield, J. Reduced moisture transport linked to drought propagation across North America. *Geophys. Res. Lett.* **46**, 5243–5253 (2019).

43. Griscom, B. W. et al. National mitigation potential from natural climate solutions in the tropics. *Philos. Trans. R. Soc. B* **375**, 20190126 (2020).

44. Chen, C., Riley, W. J., Prentice, I. C. & Keenan, T. F. CO2 fertilization of terrestrial photosynthesis inferred from site to global scales. *Proc. Natl Acad. Sci.* **119**, e2115627119 (2022).

45. Keenan, T. F. et al. Increase in forest water-use efficiency as atmospheric carbon dioxide concentrations rise. *Nature* **499**, 324–327 (2013).

46. Le Quéré, C. et al. Global carbon budget 2018. *Earth Syst. Sci. Data* **10**, 2141–2194 (2018).

47. Pan, Y. et al. A large and persistent carbon sink in the world's forests. *Science* **333**, 988–993 (2011).

48. Fu, Y. H. et al. Declining global warming effects on the phenology of spring leaf unfolding. *Nature* **526**, 104–107 (2015).

49. Peñuelas, J. & Filella, I. Responses to a warming world. *Science* **294**, 793–795 (2001).

50. Piao, S. et al. Plant phenology and global climate change: Current progresses and challenges. *Glob. Change Biol.* **25**, 1922–1940 (2019).

51. Angert, A. et al. Drier summers cancel out the CO2 uptake enhancement induced by warmer springs. *Proc. Natl Acad. Sci.* **102**, 10823–10827 (2005).

52. Lian, X. et al. Summer soil drying exacerbated by earlier spring greening of northern vegetation. *Sci. Adv.* **6**, eaax0255 (2020).

53. Peñuelas, J., Rutishauser, T. & Filella, I. Phenology feedbacks on climate change. *Science* **324**, 887–888 (2009).

54. Zhang, Y., Keenan, T. F. & Zhou, S. Exacerbated drought impacts on global ecosystems due to structural overshoot. *Nat. Ecol. Evol.* **5**, 1490–1498 (2021).

55. Wang, Y. & Yuan, X. Anthropogenic speeding up of South China flash droughts as exemplified by the 2019 Summer-Autumn transition season. *Geophys. Res. Lett.* **48**, e2020GL091901 (2021).

56. Sreeparvathy, V. & Srinivas, V. Meteorological flash droughts risk projections based on CMIP6 climate change scenarios. *npj Clim. Atmos. Sci.* **5**, 77 (2022).

57. Dong, J., Lei, F. & Crow, W. T. Land transpiration-evaporation partitioning errors responsible for modeled summertime warm bias in the central United States. *Nat. Commun.* **13**, 336 (2022).

58. Zhao, M., Liu, Y. & Konings, A. G. Evapotranspiration frequently increases during droughts. *Nat. Clim. Change* **12**, 1024–1030 (2022).

59. Fischer, E., Sippel, S. & Knutti, R. Increasing probability of record-shattering climate extremes. *Nat. Clim. Change* **11**, 689–695 (2021).

60. Noguera, I., Vicente-Serrano, S. & Domínguez-Castro, F. The rise of atmospheric evaporative demand is increasing flash droughts in Spain during the warm season. *Geophys. Res. Lett.* **49**, e2021GL097703 (2022).

61. Martens, B. et al. GLEAM v3: satellite-based land evaporation and root-zone soil moisture. *Geosci. Model Dev.* **10**, 1903–1925 (2017).

62. Hersbach, H. et al. The ERA5 global reanalysis. *Q. J. R. Meteorol. Soc.* **146**, 1999–2049 (2020).

63. Li, M., Wu, P. & Ma, Z. A comprehensive evaluation of soil moisture and soil temperature from third-generation atmospheric and land reanalysis data sets. *Int. J. Climatol.* **40**, 5744–5766 (2020).

64. Gao, J. Global 1-km downscaled population base year and projection grids based on the shared socioeconomic pathways, Revision 01. (NASA, 2020).

65. Ramankutty, N., Evan, A. T., Monfreda, C. & Foley J. A. Global Agricultural Lands: Pastures, 2000.). *NASA Socioeconomic Data and Applications Center (SEDAC)* (2010).

66. Zhao, M., Cheng, C., Zhou, Y., Li, X., Shen, S. & Song, C. A global dataset of annual urban extents (1992–2020) from harmonized nighttime lights. *Earth Syst. Sci. Data* **14**, 517–534 (2022).

67. Hansen, M. C. et al. High-resolution global maps of 21st-century forest cover change. *science* **342**, 850–853 (2013).

68. Jones, B. & O'Neill, B. C. Spatially explicit global population scenarios consistent with the Shared Socioeconomic Pathways. *Environ. Res. Lett.* **11**, 084003 (2016).

69. Nelsen, R. B. An Introduction to Copulas. Springer Science & Business Media (2007).

70. Zscheischler, J. et al. A typology of compound weather and climate events. *Nat. Rev. Earth Environ.* **1**, 333–347 (2020).

71. Schepsmeier U., et al. Statistical inference of vine copulas. Software. [Google Scholar], (2018).

72. Quade D. Nonparametric partial correlation. In: Measurement in the Social Sciences. Routledge (2017).

AUTHOR CONTRIBUTIONS

Z.Z. designed the study and conduct the analysis and wrote the manuscript. W.W., J.P., Q.G. and W.J. contributed to the interpretation of the results and revised the manuscript. Y.M., Z.L., X.R. and K.W. collected data and contributed to the manuscript preparation. All authors contributed to the manuscript writing.

COMPETING INTERESTS

The authors declare no competing interests.

ADDITIONAL INFORMATION

Supplementary information The online version contains supplementary material available at https://doi.org/10.1038/s41612-023-00468-2.

Correspondence and requests for materials should be addressed to Wenxiang Wu, Josep Peñuelas or Quansheng Ge.

Reprints and permission information is available at http://www.nature.com/reprints

Publisher's note Springer Nature remains neutral with regard to jurisdictional claims in published maps and institutional affiliations.